PRODUCTION PROCESS

Impact of wire and arc additively manufactured workpiece geometry on the milling process

Christina Fuchs[1] · **Christian Fritz**[1] · **Michael F. Zaeh**[1]

Abstract

In recent years, the wire and arc additive manufacturing (WAAM) process has been given attention as a possibility to save material during the production of large-scale parts. Drawbacks of the WAAM process are the relatively low surface quality and the low form accuracies, which require post-processing of all functional surfaces. The milling process is researched as a post-processing option, especially to achieve high form accuracies. While several authors presented successful applications of the milling process, the difficulties of machining wire and arc manufactured parts (WAAM-parts) due to the part geometry have not yet been researched. In the present research, the impact of the WAAM-part geometry on the milling process was analyzed by machining three sets of samples, and guidelines for a milling strategy were developed. The results show that the geometry leads to modulated cutting forces, whose frequency, in turn, has to be considered for the milling setup. Additionally, the modulated cutting force leads to a periodically changing deflection resulting in a form deviation on the final workpiece.

Keywords Post-processing · Ti-6Al-4V · WAAM · Cutting forces

1 Introduction

Wire and arc additive manufacturing (WAAM) may enable economical additive production of large-scale components. WAAM refers to processes where a welding power source is employed to melt a metal wire, but instead of joining two components, the melted material is deposited on a substrate, and a part is built in layers. The feasibility of the process for producing industrially relevant geometrical features was proven by [1], and its economic potential was studied by [2]. It was concluded that for the production of airfoils 59.7% of the material is savable [3]. However, a drawback of the process is the relatively low surface quality [4] and the difficulty of achieving high form accuracies. Consequently, post-processing is necessary to obtain functional surfaces. The milling process is investigated as an option to improve the surface quality and the form accuracy in one process. To successfully machine the wire and arc additively manufactured components (WAAM-components), their machinability and machining process stability have to be determined. Some research has already been conducted in this field. For example, the cutting forces, the chip formation, and the milling strategy for several WAAM-materials were studied. Overall, the results varied. For AISI H13 stainless steel, [5] found the machinability of WAAM-material to be lower than for conventionally produced material. Contrastingly, [6] concluded that the machinability of AISI 316L was similar to or slightly better than for rolled rods of the same material. For Ti-6Al-4V, [7] showed that the machinability of WAAM-material was worse than the machinability of conventional material, while the milling strategy did not influence the cutting forces [8]. Tool wear is an additional value to measure machinability. On this subject, [9] reported significant tool wear while milling wire and arc manufactured HSLA steel. The authors linked this to the non-homogeneous microstructure of the material. Finally, the process stability of the milling process was analyzed by [10]. Reference [10] determined that WAAM process parameters influence the chatter behavior of walls since the geometry and the mechanical properties are influenced by the process parameters.

The geometry of the WAAM-parts has already been the research focus of several studies. While most authors studied

✉ Christina Fuchs
christina.fuchs@iwb.tum.de

Christian Fritz
christian.fritz@iwb.tum.de

Michael F. Zaeh
michael.zaeh@iwb.tum.de

1 Institute for Machine Tools and Industrial Management, Technical University of Munich, Boltzmannstrasse 15, 85748 Garching, Germany

single-bead with single-layer deposition (for example [11]), some researched multi-layer parts. Of those studying multi-layer deposition, [12] showed that an oscillatory strategy resulted in better flatness values than parallel deposition of beads. Concerning the resulting surface profile of deposited parts, [13] studied the influence of cooling methods on the wall geometry. They determined a minimum waviness of 0.6 mm of their single bead, multi-layer deposit, corresponding to the layers of the deposited material. That the waviness corresponds to the deposition strategy was also concluded by [4], who studied the surface profile of multi-layer parts deposited with a 'zig-zag' strategy. A similar strategy, called the 'weave' strategy, was analyzed by [14]. The authors concluded that the strategy is especially applicable for large-scale structures. Since the benefit of wire and arc additive manufacturing is especially high for large-scale structures, the objective of the present research was to determine the impact of the WAAM-part geometry deposited by oscillating strategies on the milling process and to develop guidelines for the milling of WAAM-parts to prevent catastrophic process failures.

2 Methods

To determine the impact of the WAAM process on the milling process, nine WAAM-samples in three sets of three each were manufactured and milled. The cutting forces and the resulting surface qualities were analyzed. Based on the findings, guidelines for the milling of WAAM-parts were developed. Two sets were manufactured from Ti-6Al-4V and one from AlSi10Mg. The planned geometry of the samples was identical in length and height, but the width differed to show the different surface profiles developing while depositing different widths of material.

2.1 Wire and arc additive manufacturing

The deposition strategy for each sample set is shown in Fig. 1, while the welding parameters are listed in Table 1. The deposition of the sample set I (SI) was performed with a WAAM setup consisting of a Yaskawa MH24 robot (Yaskawa Denki, Kitakyūshū, Japan) with a welding torch mounted and a Fronius TPSi welding power supply (Fronius International GmbH, Pettenbach, Austria). The deposition took place in an ambient atmosphere. Sample set II (SII) and III (SIII) were manufactured on a second WAAM setup at the Institute for Machine Tools and Industrial Management (Technical University of Munich). The setup consists of a Fronius TPS welding power supply and the welding torch mounted on a Kuka Robot (Kuka AG, Augsburg, Germany). Due to the high oxidation rate of Ti-6Al-4V, the deposition took place in an inert argon atmosphere. All substrate plates had the identical dimensions of 140 mm × 100 mm × 6 mm. The orientation of the deposited wall was along the longest side of the substrate plate. The wall itself had a length of 80 mm and the number of layers was chosen so that the resulting
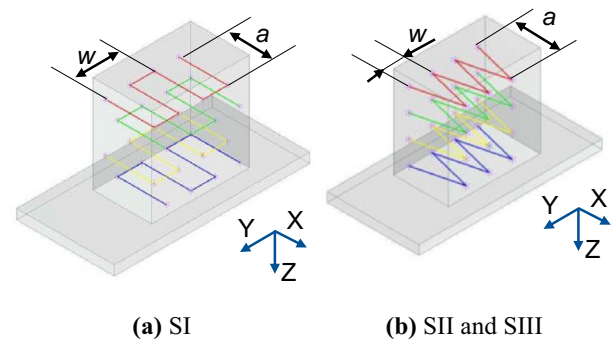
(a) SI **(b)** SII and SIII

Fig. 1 Deposition strategies for the samples; the line colors serve to improve the visibility

Table 1 Welding setup and parameters for the wire and arc manufacture of the samples

	SI	SII	SIII
Material	AlSi10Mg	Ti-6Al-4V	Ti-6Al-4V
Wire speed v_D in mm/min	2.2	6.5	8.0
Torch speed v_T in mm/min	800	650	800
Setup	TPSi	TPS	TPS
Wire diameter in mm	1.6	1.2	1.2
Substrate material	AlMg3	Ti-6Al-4V	Ti-6Al-4V
Amplitude a in mm	18.85	12.00	7.00
Wavelength w in mm	6.3	4.0	4.0
Number of waves	12	20	20
Number of layers	31	8	8

height was roughly 40 mm. As seen in Fig. 1, the Z-axis corresponds to the building direction, while the Y-axis corresponds to the welding direction.

2.2 Milling experiments

The milling experiments were conducted on a GROB 352T machining center (Grob Werke GmbH, Mindelheim, Germany). Each sample was mounted on a 3-axis dynamometer (Type 9257B, Kistler Group, Winterthur, Switzerland) with an adapter plate to measure the cutting forces during machining. Machining was performed using end mills with a 16 mm diameter. Before the measurements, the X–Y surface of the parts was milled to keep the axial engagement stable during the measurements. The steps of the milling process are depicted in Fig. 3. Figure 3a shows the initial setup of the part. The part after the removal of the X-Y surface is depicted in Fig. 3b. On the SII and SIII the start and end zone were removed, to keep passes without cutting on the middle of the workpiece to a minimum. A part after the removal of the start and the end zone is shown in Fig. 3c.

Feed direction paralleled the Y-axis of the dynamometer. Therefore, the tool's axial direction was parallel to the
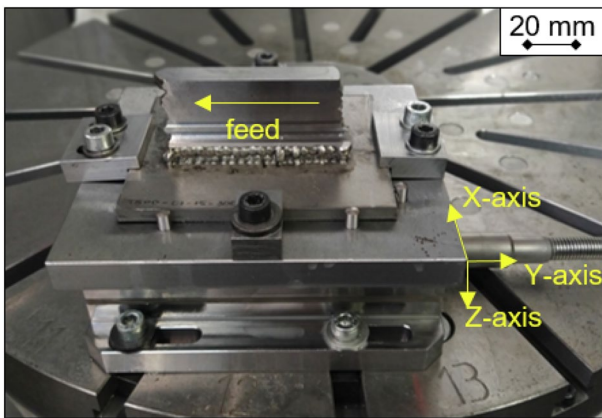
Fig. 2 Milling setup

Table 2 Machining and tool parameters

	SI	SII	SIII
Material	AlSi10Mg	Ti-6Al-4V	Ti-6Al-4V
Cutting speed v_c in m/min	200	55	55
Feed v_f in mm/min	597	88	88
Radial engagement a_e in mm	3.15	1.00	1.00
Axial engagement a_p in mm	32	28	28
Tool diameter in mm	16	16	16
Number of teeth	4	4	4
Corner radius in mm	0	4	4
Cutting Material	Solid Carbide	Solid Carbide	Solid Carbide
Coating	TiAlN	TiAlN	TiAlN
Flood coolant	On	On	On
Cutting length in mm	36	32	32

dynamometer's Z-axis and the tool's radial direction paralleled the X-axis. Figure 2 depicts the milling setup and the axis orientations. The sampling frequency was 20,000 Hz.

Cutting passes along the surface were conducted until a deposited surface was no longer visible. On the SI, this depth of cut was reachable with one cut. On the SII and SIII, several cuts were necessary. After the even surface was reached, surface measurements were performed. In Table 2, the machining parameters are given.

2.3 Measurement strategy

After the WAAM process, the samples were scanned with a 3D scanner (Comet L3M, Steinbichler Optotechnik GmbH, Neubeuern, Germany) and a CAD model for each of the deposited parts was obtained. Before and after the milling process, the samples' Y-Z-surfaces were digitized with a profilometer VK-3100 (Keyence Corporation, Osaka, Japan). The waviness and roughness were determined based on the digitized surfaces. The cut-off wavelengths of the roughness λ_c and the waviness λ_f for the measurements are given in Table 3.

3 Results and Discussion

3.1 Part geometry before milling

The geometries of the three sample sets differed strongly before the machining process. In Figure 4, a detail of the surface from each sample set is depicted. The mean values and the standard deviation of the surface roughness and waviness parameters are given in Table 5 in the appendix. The mean width of the waviness profile (Wsm) in the Y-direction corresponds on all sample sets to the wavelength of the deposition strategy. On SI, the mean arithmetic waviness Wa and the maximum waviness Wt in the Y-direction exceed the corresponding values in the Z-direction. This result is opposite to the SII and SIII, where the waviness in the Z-direction exceeds the waviness in the Y-direction. On all sample sets, the waviness exceeds the roughness. Therefore, the waviness is likely to more strongly influence the milling process.
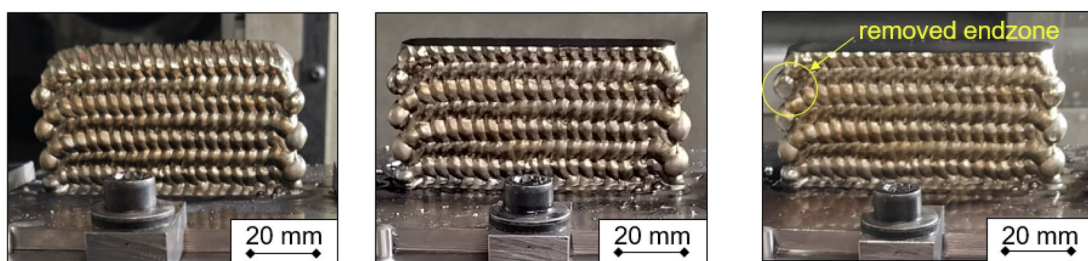
(a) initial part　　　**(b)** after removing the top layers　　**(c)** after removing the start and the end zone

Fig. 3 The steps of the milling process, exemplarily depicted for sample set II; step (c) is optional and was not performed on SI, since no significant start and end zone were detected on those samples

Table 3 Measurement parameters

In mm	Before machining	After machining
λ_c	0.8	0.8 (SI) and 2.5 (SII, SIII)
λ_f	2 (SI) and 8 (SII, SIII)	80

3.2 Cutting forces

In Fig. 5, the moving average of the cutting forces in the radial and the feed direction for each sample set is depicted. It was calculated over one spindle rotation. For SI, only one pass was necessary to remove the waviness. Multiple passes were conducted for SII and SIII.

For SI, there is a visible incline in the forces. This incline is attributable to a positioning error during the deposition process. It results in a positioning error in the machine tool and, therefore, in a rising radial depth of cut during the milling process. Otherwise, the moving average forces have a modulation with a time interval of roughly 0.63 s. Considering the feed speed, the modulation length is 6.3 mm. It corresponds to the Wsm-value in the Y-direction of the samples. The feed force was lower than the radial force. This can be explained by the cutting parameters.

For SII, the first pass was without engagement. Therefore, no cutting forces were measured. Within the second pass, the start and end zone were cut. On the third pass, the tool was engaged along the whole surface. The actual engagement rises through the 4th, 5th, 6th, and 7th pass. The part was visually inspected after the 7th pass. The surface resulting from the WAAM process was completely removed, and cutting was stopped. Overall, the cutting forces increased with the passes. They varied significantly within the first few passes, while the level remained nearly constant during the 6th and 7th pass. The modulation of the moving average is not as periodic as for the SI, but the length once again corresponds to the Wsm-value in the Y-direction.

For SIII, the modulation of the moving average is not visibly periodic. The mean and the maximum waviness for these samples were much lower than for SI and SII, which probably result in the undetectable periodicity, even though the Wsm-value of the unmilled WAAM-surface corresponds to the deposition strategy.

A Fourier transformation was performed on the force signals to prove that the periodicity of the cutting forces corresponds to the waviness of the parts. In Fig. 6, the results of the Fourier transformation are depicted. On each sample, the tooth engagement frequency, at 266.67 Hz for SI and 73.30 Hz for SII and SIII, was present as a peak in the data. The tooth engagement frequency is calculated from the number of teeth z and the spindle speed n by

$$f_{tooth} = \frac{z}{n}. \tag{1}$$
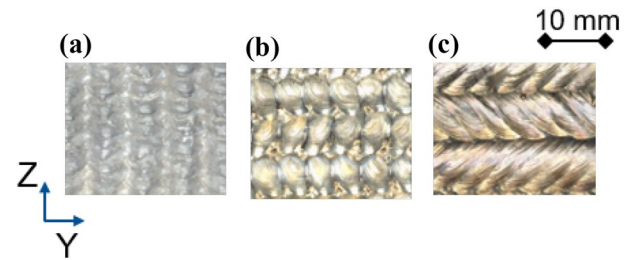
Fig. 4 Surfaces before machining, **a** SI, **b** SII, **c** SIII

Additionally, the spindle rotational frequency, at 66.67 Hz for SI and 18.30 Hz for sample set II and III, was detectable. It is the inverse of the spindle speed.

Notably, on SI and SII, an additional peak was identified at 1.57 Hz for the SI and 0.36 Hz for SII. It corresponds to the theoretical frequency of the cutting force modulation. When the waviness in the feed direction is assumed to be periodic, it is characterized by its wavelength l_w and its form. In turn, the angle of immersion and the contact length of the tool become a periodic function of the wavelength and the form. This in turn leads to the periodically modulated cutting forces, with a modulating frequency of

$$f_w = \frac{v_f}{l_w}, \tag{2}$$

where v_f denotes the feed speed in mm/min. The calculation leads to a modulation frequency of 1.58 Hz for SI, corresponding to the measured value.
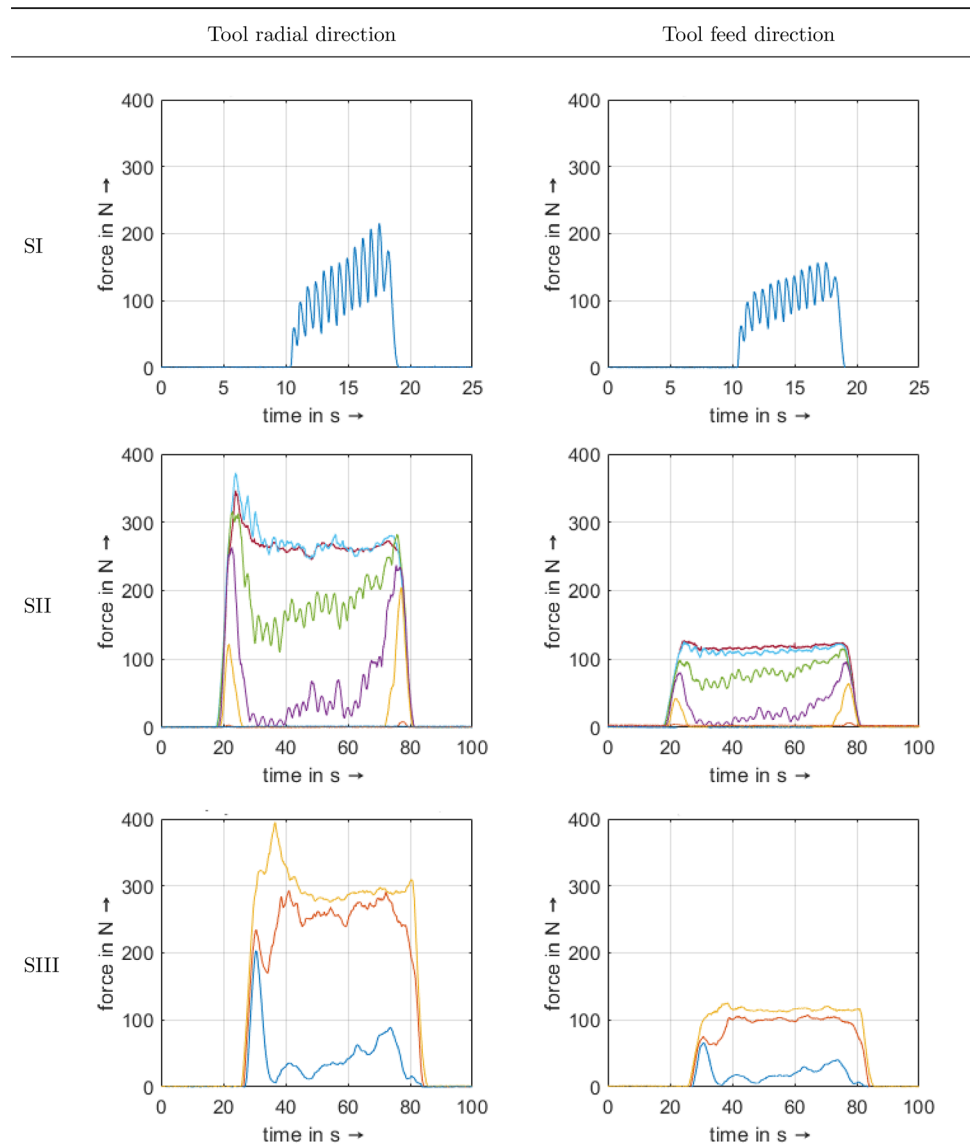
3.3 Resulting surface quality

The surface quality of the three sample sets strongly differs after the milling process. In Table 6 in the appendix, the mean surface roughness and waviness for all sample sets are listed.

Notably, the Wsm-value in the Y-direction on SI has not significantly changed compared to the surface before machining. It still corresponds to the WAAM strategy, even though the parts were milled until the deposited surface was completely removed. Contrastingly, on SII and SIII, the Wsm-value no longer corresponds to the WAAM strategy.

Overall, the maximum roughness Rt on the SI is lower than on the SII and SIII. At the same time, its maximum waviness exceeds the waviness on SII and SIII. No discernible difference between the surface roughness and the waviness was detected between SII and SIII. This shows conclusively that, with different deposition parameters, the same surface quality is achievable. Since both sample sets were milled with identical parameters, it also indicates that the influence of the deposition

Fig. 5 Moving average force: the moving average was calculated over the length of one spindle rotation; —1st pass, —2nd pass, —3rd pass, —4th pass, —5th pass, —6th pass, —7th pass

parameters and strategy on the surface quality after the milling process were negligible in this case.

3.4 Discussion

The presented results also reveal some limitations, however. The engagement ratio during the machining depends on the raw part geometry. Due to the sequential process chain, uncertainties in the WAAM process have a direct effect on the subsequent machining. A high variation in the waviness could be observed between individual WAAM-samples, both between the sample sets and within each sample set. The relatively high standard deviations in Table 5 attest to that. Despite several models for stock modeling of WAAM-parts already described in literature, high uncertainties continue to occur in the assumption of a stock geometry. Therefore, our model for the milling process is
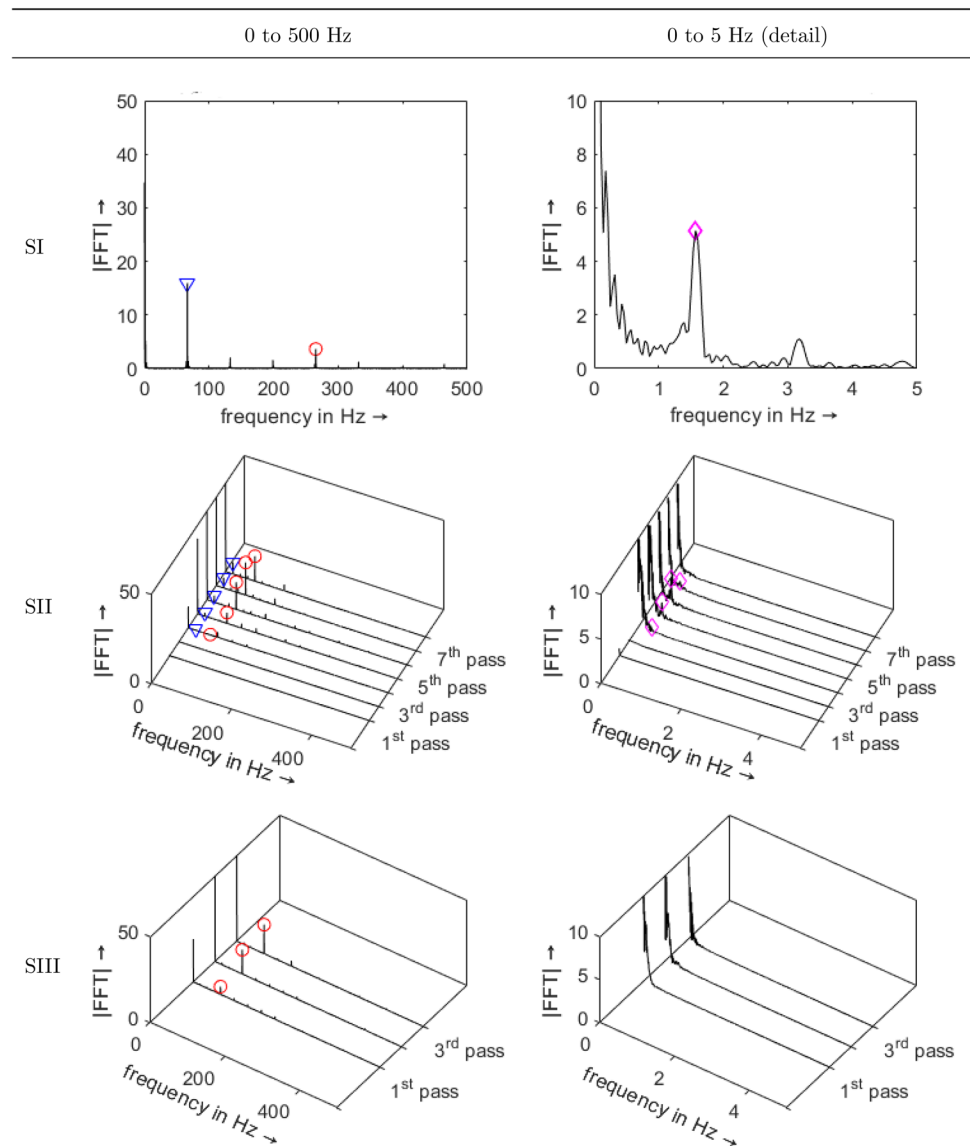
affected by the intersample and intrasample deviations caused by the WAAM process.

In addition, the measurement of forces using a force measurement platform is a major challenge. There is a constantly changing multidimensional load on the cutter and thus there are high vibrations in the process due to the shape deviations already discussed. These have an unfavorable effect on the measurement of the individual cutting forces. In addition, the definition of the axes in the process presents a great difficulty. Since no component has a clear axis, a robust calibration method must be found that allows small deviations in the axes definition. Using our method, similar to zero-point clamping, the error could be reduced, but there is still a residual uncertainty between samples.

An increased waviness after machining between sample sets SII and SIII was observed (see Table 6 in the appendix). This difference might be explainable by the smaller wall thickness of

Fig. 6 Fast Fourier transformation of the cutting force in the tool's radial direction, ○tooth

engagement frequency, ▽ spindle rotational frequency, ◇ modulating frequency

4 Impact on the milling process

Two challenges were identified from the experimental results concerning the WAAM-material: forced vibrations due to the modulating frequency of the cutting forces and form errors resulting from irregular deflections. Both are addressed in the following sections and guidelines for a milling strategy are proposed.

the struts of SIII and thus an increased susceptibility to vibration. However, our results show that a surface quality sufficient even for functional surfaces was achievable in both cases.

4.1 Forced vibrations

Forced vibrations with high amplitudes occur when the frequency of the cutting force matches the natural frequency of the machine tool or the workpiece (resonance) [15], in this case, the tooth engagement and spindle frequencies as well as the modulating frequency. The natural frequencies are obtainable by modal testing [15] from the frequency response function (FRF).
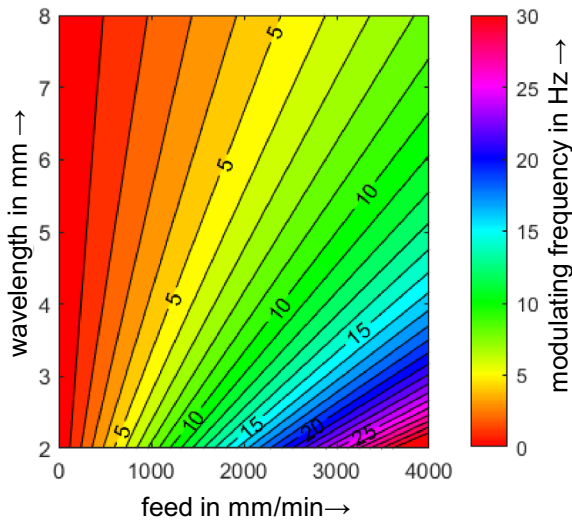
Fig. 7 Modulating frequency of the mean cutting force

In Fig. 7, the modulating frequency over the wavelength and the feed for a tool with four teeth is depicted.

Depending on the wavelength and the feed speed, the modulating frequency can reach values of 15 Hz or more. For low spindle rotational speeds, it might even coincide with the spindle rotational frequency leading to a significant amplitude of the force and a possible excitation of the workpiece, the tool, or the machining setup. It is unlikely that a problem would arise for small parts and tools, as used in this study. For larger structures and tools, this excitation should be considered. Often, post-processing of the WAAM-components with an industrial milling robot is discussed. For industrial milling robots, eigenfrequencies of the first mode at 5.5 Hz [16], at 8.4 Hz [17] and around 10 Hz [18] have been reported. In this case, the modulating frequency could coincide with a structural eigenfrequency, which could lead to strong forced vibrations. Additionally, the cutting with a changing radial engagement, especially if the change is periodical, results in a modulation of the chip thickness and could lead to chatter or other vibration phenomena.

4.2 Deflections

On SI in the Y-direction, a Wsm-value corresponding to the deposition strategy was detected, even though the deposited surface was completely removed. At the same time, the maximum waviness Wt was higher than on the other samples. A likely reason for these results is an irregular deflection of the tool and the workpiece due to the modulation of the mean cutting force.

To show this, the maximum deflections of the tool and the workpiece due to the modulation of the mean cutting force were calculated for SI. In theory, the Wt-value should then correspond to the difference in the deflection calculated along the pass. For the calculation, the tool was modeled as a cantilever beam with a cylindrical shape [19]. The concentrated forces were used with the equation for the tool deflection d_T given by [15]

$$d_T = \Delta F / k, \tag{3}$$

where F denotes the cutting force and k the static stiffness of the tool clamped in the spindle. Since the clamping in the spindle is usually much stiffer than the tool, the equation was simplified to

$$d_T = \frac{\Delta F \cdot l^3 \cdot 64}{3 \cdot E \cdot \pi \cdot D_e^4}, \tag{4}$$

where l is the distance from the collet to the tooltip, E is the Young's modulus of the cutter, and D_e is the effective cutter diameter. With a Young's modulus of 600,000 N/m² for the tool, the measured forces during the cutting of SI and l at 35 mm, the maximum deflection of the tool d_T is estimated to be $9.1 \pm 0.7 \, \mu m$.

For the deflection of the workpiece, the workpiece was assumed to be a cuboid with constant stiffness, independent of the material removal. It is an acceptable assumption if the amount of material removed is small. While disregarding the beginning and end of the part, the maximum deflection was estimated by the deflection of a rectangular beam under a constant force. The workpiece deflection d_W is then equal to

$$d_W = \frac{\Delta F \cdot h^3 \cdot 4}{E \cdot l \cdot w_{eff}^3}, \tag{5}$$

where F denotes the force, E the Young's modulus of the workpiece, h the length of the part, and w_{eff} the remaining width of the part. With a Young's modulus of 70,000 N/m² for aluminium and a remaining width of the part of 18.85 mm, the workpiece deflection was estimated to be between 2.3 and 3.4 µm. In Table 4, the estimated deflections based on the measured maximum forces in the tool's radial direction for each sample of SI are given. The measured maximum waviness Wt is $15.48 \pm 2.52 \, \mu m$. The calculated deflections are lower than the measured maximum

Table 4 Estimated deflections

In µm	SI No. 1	SII No. 2	SIII No. 3
d_T	6.2 ± 1.2	9.1 ± 0.7	8.6 ± 1.3
d_W	2.3 ± 0.4	3.4 ± 0.3	3.2 ± 0.5

waviness. The calculated deflections, based on the cutting forces, should underestimate the actual deflection, since as soon as deflection occurs, the cutting forces decrease. The measured cutting forces are therefore lower, than the forces leading to the deflection would have been.

4.3 Guidelines for the milling process

Based on the experimental results and the theoretical considerations of the impact of the WAAM-geometry on the milling process, the following guidelines for the milling process planning were developed:

1. To keep the mean cutting forces as stable as possible, keep the feed direction in the direction of the smaller waviness.
2. Ensure that the modulating frequency and the rotational frequency of the spindle are not identical. This occurs for low spindle speeds.
3. The modulating frequency and its harmonics might induce forced vibrations. Therefore, design the setup and clamping so that no natural frequency coincides with the modulating frequency.
4. The force modulation leads to changing deflections. Design the milling process so that a minimal force variation occurs on the surface defining cut.

5 Conclusion

This research had the objective of determining the impact of the WAAM-component geometry on the milling process and developing guidelines for the milling process planning. Therefore, three sets of WAAM-samples were manufactured from AlSi10Mg and Ti-6Al-4V, representing different component characteristics. The geometry was specified by optical surface roughness and waviness measurements. Next, the samples were milled with peripheral milling, and the cutting forces were determined. The resulting surface quality was measured optically as well. The key findings of the research were:

- The geometry of the samples is related to the deposition strategy. For a periodic deposition strategy, a periodic surface profile emerges. Then, the Wsm-value in the welding direction corresponds to the deposition strategy.
- The mean cutting force displays the same periodicity as the surface profile. This modulation might lead to a force excitation of the milling process.
- The cutting force modulation can result in periodically changing deflections of the workpiece and the tool. On parts

with low stiffness and only one cutting pass, it might lead to flatness errors (unevenness) of the finished component.

- For the milling process planning, the expected modulation frequency should be considered. The setup and the clamping should be designed accordingly. A finishing pass should be implemented to counteract the periodic deflections.

Some challenges were encountered while performing this research. Firstly, the welds often produce a start and an end zone. On the WAAM-components in this research, the zones protruded from the additively manufactured walls. They had to be removed before the measurements to prevent critical tool engagement and prolonged cuts without material removal. In the future, these start and end zones have to be considered for the milling strategy. Secondly, locating the WAAM-components with measuring probes in the machine tool is challenging due to the distortion of the substrate plate and the uneven surface profile of the welded component. Fixed clamping, with the welding and the milling positions similar to a zero-point clamping system, countered this effect within this research. Even so, for one sample set a positioning error occurred, resulting in a rising radial engagement along the cut. For the industrial application of the process chain, a clamping strategy should be developed to enable secure positioning for both processes. Serial production of WAAM-components would benefit most from this solution. For one-piece production, another solution might be the digitization of the component in its clamping position in the machine tool and tool path planning based on this digitized model.

Several aspects were not addressed within this research, but seem especially important for future research. Firstly, all results in this study were obtained by experiments on one geometrically simple shape. Industrial parts consist of a combination of simple shapes and complex features. Therefore, it should be studied how the proposed milling strategy guidelines can be applied to industrial parts and how the milling process of complex features is influenced by the WAAM-geometry. Secondly, the periodicity of the surface profile results essentially in a modulation of the chip thickness, similar to the conditions leading to the chatter phenomena. Therefore, it should be studied whether chatter theory applies to the process and whether it could lead to economic gains for the machining process. Thirdly, changing tool engagements place an additional stress on the tool. Accordingly, the tool wear mechanism should be investigated, since tool wear is relevant for the economic application of machining processes.

Appendix A: Surface roughness

See Tables 5 and 6

Table 5 Surface quality before machining (mean value and standard deviation)

Y-axis | Z-axis	Unit	SI	SII	SIII
Ra	µm	6.01 ± 0.19 | 6.90 ± 0.12	19.89 ± 2.09 | 26.23 ± 2.15	2.88 ± 0.72 | 6.58 ± 0.10
Rt	µm	111.55 ± 6.41 | 89.73 ± 15.36	699.10 ± 154.43 | 1052.20 ± 94.24	121.67 ± 96.86 | 197.54 ± 19.56
Rsm	µm	– | –	– | –	– | –
Wa	µm	344.81 ± 17.24 | 107.18 ± 9.08	196.02 ± 8.25 | 260.93 ± 8.15	55.06 ± 4.60 | 130.80 ± 2.32
Wt	µm	1564.43 ± 48.87 | 685.21 ± 163.98	1195.09 ± 88.84 | 1617.15 ± 115.17	345.03 ± 56.62 | 725.81 ± 38.30
Wsm	µm	6438.23 ± 14.58 | 5489.62 ± 199.80	3947.17 ± 19.72 | 5211.31 ± 227.52	4185.52 ± 48.83 | 4911.20 ± 97.41

Table 6 Surface quality after machining (mean value and standard deviation)

Y-axis | Z-axis	Unit	SI	SII	SIII
Ra	µm	0.20 ± 0.01 | 0.20 ± 0.01	0.27 ± 0.02 | 0.31 ± 0.04	0.31 ± 0.05 | 0.35 ± 0.01
Rt	µm	4.85 ± 1.94 | 3.66 ± 0.95	6.71 ± 5.29 | 5.02 ± 1.71	8.14 ± 6.48 | 3.72 ± 0.74
Rsm	µm	– | 335.06 ± 0.04	705.96 ± 14.61 | 629.08 ± 23.53	730.16 ± 17.15 | 712.68 ± 19.98
Wa	µm	3.14 ± 0.27 | 01.6 ± 0.09	0.66 ± 0.11 | 3.12 ± 0.07	1.61 ± 0.21 | 4.92 ± 0.33
Wt	µm	15.48 ± 2.52 | 8.08 ± 0.91	4.71 ± 1.22 | 11.46 ± 0.46	10.40 ± 1.65 | 20.17 ± 1.16
Wsm	µm	6485.98 ± 129.27 | 11462.95 ± 550.93	19021.90 ± 5454.40 | 14685.29 ± 264.45	34672.15 ± 2898.83 | 15161.54 ± 129.23

References

1. Kazanas P, Deherkar P, Almeida P, Lockett H, Williams S (2012) Fabrication of geometrical features using wire and arc additive manufacture. Proc Inst Mech Eng Part B J Eng Manuf 226(6):1042–1051
2. Martina F, Williams S (2015) Wire + arc additive manufacturing vs. traditional machining from solid: a cost comparison
3. Campatelli G, Montevecchi F, Venturini G, Ingarao G, Priarone PC (2020) Integrated WAAM-subtractive versus pure subtractive manufacturing approaches: an energy efficiency comparison. Int J Precis Eng Manuf Green Technol 7(1)
4. Fuchs C, Baier D, Semm T, Zaeh MF (2020) Determining the machining allowance for WAAM parts. Prod Eng Res Devel 14(5–6):629–637

5. Montevecchi F, Grossi N, Takagi H, Scippa A, Sasahara H, Campatelli G (2016) Cutting forces analysis in additive manufactured aisi h13 alloy. Proc CIRP 46:476–479 (**7th HPC 2016—CIRP conference on high performance cutting**)

6. Masek P, Fornusek T, Zeman P, Bucko M, Smolik J, Heinrich P (2019) Machinability the aisi 316 stainless steel after processing by various methods of 3D printing. MM Sci J 3338–3346:2019

7. Alonso U, Veiga F, Suárez A, Artaza T (2020) Experimental investigation of the influence of wire arc additive manufacturing on the machinability of titanium parts. Metals 10(1)

8. Veiga F, Del Val AG, Suárez A, Alonso U (2020) Analysis of the machining process of titanium Ti-6Al-4V parts manufactured by wire arc additive manufacturing (WAAM). Materials 13(3)

9. Lopes JG, Machado CM, Duarte VR, Rodrigues TA, Santos TG, Oliveira JP (2020) Effect of milling parameters on HSLA steel parts produced by wire and arc additive manufacturing (WAAM). J Manuf Process 59:739–749

10. Chernovol N, Sharma A, Tjahjowidodo T, Lauwers B, van Rymenant P (2021) Machinability of wire and arc additive manufactured components. CIRP J Manuf Sci Technol 35:379–389

11. Benakis M, Costanzo D, Patran A (2020) Current mode effects on weld bead geometry and heat affected zone in pulsed wire arc additive manufacturing of Ti-6-4 and Inconel 718. J Manuf Process 60:61–74

12. Aldalur E, Veiga F, Suárez A, Bilbao J, Lamikiz A (2020) Analysis of the wall geometry with different strategies for high deposition wire arc additive manufacturing of mild steel. Metals 10(7):1–19

13. Corradi DR, Bracarense AQ, Wu B, Cuiuri D, Pan Z, Li H (2020) Effect of Magnetic Arc Oscillation on the geometry of single-pass multi-layer walls and the process stability in wire and arc additive manufacturing. J Mater Process Technol 283

14. Li Z, Ma G, Zhao G, Yang M, Xiao W (2018) Weave bead welding based wire and arc additive manufacturing technology. In: Wang S, Price M, Lim MK, Jin Y, Luo Y, Chen R (eds) Recent advances in intelligent manufacturing, vol 923. Springer, Singapore, p 408

15. Altintas Y (2012) Manufacturing automation, 2nd edn. Cambridge University Press, Cambridge

16. Denkena B, Bergmann B, Lepper T (2017) Design and optimization of a machining robot. Proc Manuf 14:89–96

17. Bauer J, Friedmann M, Hemker T, Pischan M, Reinl C, Abele E, von Stryk O (2013) Analysis of industrial robot structure and milling process interaction for path manipulation. In: Denkena B, Hollmann F (eds) Process machine interactions. Lecture notes in production engineering. Springer, Berlin, pp 245–263

18. Busch M, Zaeh MF (2022) Multi-fidelity information fusion to model the position-dependent modal properties of milling robots. Robotics 11(1)

19. Dépincé P, Hascoët J (2006) Active integration of tool deflection effects in end milling. Part 1. Prediction of milled surfaces. Int J Mach Tools Manuf 46(9):937–944